# Experimental Validation of Above-Floor Tube-and-Plate Radiant Floor Model

Sébastien A. Brideau[1], Ian Beausoleil-Morrison[1], Michaël Kummert[2]
[1]Department of Mechanical and Aerospace Engineering, Carleton University, Ottawa, Canada
[2]Department of Mechanical Engineering, Polytechnique Montréal, Montréal, Canada

## Abstract

This paper discusses the experimental validation of a new above-floor tube-and-plate radiant floor model. It describes the experiments that were designed and conducted and the instrumentation employed, and then contrasts the measurements with model predictions. The sensitivity of model predictions to uncertain inputs is also treated. Overall, the experimental results were found to be in close agreement with the model. This contribution represents the first known experimental validation of a working above-floor tube-and-plate radiant floor model that is suitable for use in building performance simulation tools.

## Introduction

Hydronic radiant floor heating and cooling have the advantage of using milder water temperatures than other types of heating or cooling systems. Energy savings can result from these milder water temperatures because the heating (or cooling) generation equipment can usually perform more efficiently and because low-temperature solar systems can be utilized. To be able to accurately predict the performance of hydronic radiant floor systems, accurate models are required. Models are readily available in various building simulation packages for embedded-tube systems (Brideau et al., 2016). Figure 1 shows a section of a typical embedded-tube thin slab radiant floor. Hot water is pumped through the tubes during periods of heating demands and the heat diffuses through the gypsum up to the floor covering. The heat is then radiated and convected in the space. Similarly, during periods of cooling demand, cold water is pumped through the floor tubes. Embedded tube systems are heavier and may require a larger structure to support the extra weight. Additionally, because of the large thermal mass in typical embedded-tubes radiant floors, controls can be more complex (Athienitis and Chen, 2000).

Above-Floor Tube-and-Plate (AFTP) systems can be used instead of embedded-tube systems to reduce thermal mass. Figure 2 shows a cross-section of an AFTP radiant floor. These systems consist of a thin conductive fin on top of a grooved high density insulation layer. The insulation layer is above a wooden

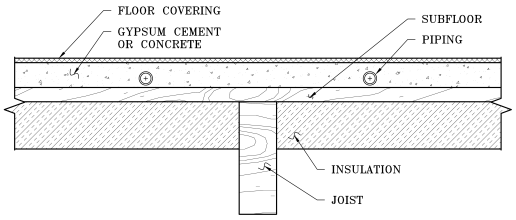


*Figure 1: Embedded tubes radiant floor*

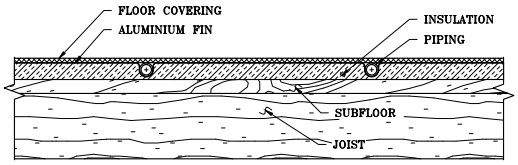


*Figure 2: AFTP floor with tube in high density insulation*

subfloor. Tubes are laid in the grooves, and a floor cover is added on top. An alternative design is to use a grooved wooden subfloor and place the insulation below the subfloor. Models for these types of radiant floors are however not currently available in Building Performance Simulation (BPS) software. This paper discusses the experimental validation of a model developed for ESP-r. The model development and preliminary verification with a finite element model were presented by Brideau and Beausoleil-Morrison (2014).

### Previous works

The literature on AFTP models is minimal. Yeo and Kim (1997) developed a model for a fin radiant floor panel. The model consisted of two layers of insulation, underneath a fin. This arrangement is very sim-

ilar to a AFTP system, except that there was no floor cover. They modeled the floor using the finite difference method with an implicit scheme, but it is not clear how the tube was modeled and coupled to the finite difference model. Additionally, the model was not implemented in a building performance simulation tool. Surface temperatures between the model and experimental results are reported to generally agree to within 0.5 °C.

Kattan et al. (2012) developed an AFTP radiant floor model that used finite difference in the water flow direction. A fin was used at the bottom of the concrete layer to increase conduction. This model used a fin thermal resistance to calculate the heat transferred to the room. The fin thermal resistance was based on steady-state fin equations. The results were compared with transient experimental results by Cho and Zaheer-uddin (1997). After review of the results provided in the paper, it is the opinion of the authors of the present paper that the model does not agree with the experimental results. Additionally, there are problems with the way errors are reported, specifically, percentage errors are reported for temperature measurements.

Brideau and Beausoleil-Morrison (2014) developed an AFTP model for ESP-r, and verified it with a FEA model. This model was based on a 2D finite difference solution, coupled with an analytical solution for the tube (Laouadi, 2004). The AFTP model and the FEA model showed very good agreement.

## Experimental validation

The inter-model comparison described by Brideau and Beausoleil-Morrison (2014) can only verify certain aspects of the model. For example, the finite element model was not equipped to deal with the flow rate and longwave radiation, so idealized conditions were simulated. In order to further verify the ESP-r model under real conditions, an experiment was conducted in the Urbandale Centre for Home Energy Research on the Carleton University campus. The objective of the experiment was to predict the experimental conditions (mainly heat transfer rate between water and floor, and floor top surface heat flux) in ESP-r given a set of inputs (including supply temperature and flow rate). The heat transfer rate between the water and the floor is defined as the product of the mass flow rate of water through the tube and the change in specific enthalpy of the water between the inlet and outlet of the radiant floor loop. The top surface heat flux is the sum of the convective and radiative heat transfer rate between the floor to the room above per floor area. The middle bedroom of the second floor was instrumented. This room was used because of its small size and the simple geometry of the serpentine layer in the floor, making it simpler to instrument and analyze.

*Table 1: Construction of floor*

| Material | Thickness ($m$) |
|---|---|
| Gypsum Board | 0.013 |
| Air space | 0.305 |
| Plywood Subfloor | 0.016 |
| Roth Panel[a] | 0.025 |
| Mortar | 0.003 |
| Cement Backing Board | 0.006 |
| Mortar | 0.003 |
| Tile | 0.009 |

[a] Roth panel is made of High Density Insulation overlaid with an aluminium sheet (0.0005 $m$ thick). Tubes are located in grooves in Aluminium sheet.

**Experimental apparatus**

The floor construction is shown in Table 1. The PEX tubes have a spacing of 0.152 m.

Twelve thermocouples were installed on the floor surface. These were organized in pairs of two; one above the tubes and one between the tubes. Due to measurement quality issues, only thermocouples 1B through 6A were used. Seven thermocouples with aspirated radiation shields (as per design by Tarara and Hoheisel (2007)) were installed at various locations in the space to get an accurate measurement of average room air temperature. Two Hukseflux HFP01 heat flux sensors were installed on the floor surface, near the centre of the room; one above the tube and one between the tubes. The heat flux meters consist of calibrated thermopiles within a thin thermally conductive puck of known thermal conductivity. The heat flux across the sensor creates a small temperature difference across the thermopile, which then creates a $mV$ signal proportional to the heat flux. The manufacturer has calibrated each individual heat flux sensor and provides a sensitivity coefficient for each of them. Figure 3 shows the location of the instruments described above.

Two thermocouples and two heat flux sensors were installed under the subfloor, approximately in the center of the floor. One set of thermocouples and heat flux sensor was located between tubes and the other directly below the tube. The underside of the gypsum board (the bottommost layer of the floor construction; located in the room below), was also equipped with a single thermocouple and heat flux meter. The installation of these sensors occurred from underneath the radiant floor construction. Additionally, thermocouples and Hukseflux HFP01 heat flux sensors were installed on the walls, ceiling, and window.

The spool with which thermocouples were made was calibrated by Johnson (2011). The uncertainty for thermocouples considering all sources was 0.47 °C. The sources of uncertainty for the thermocouple cali-

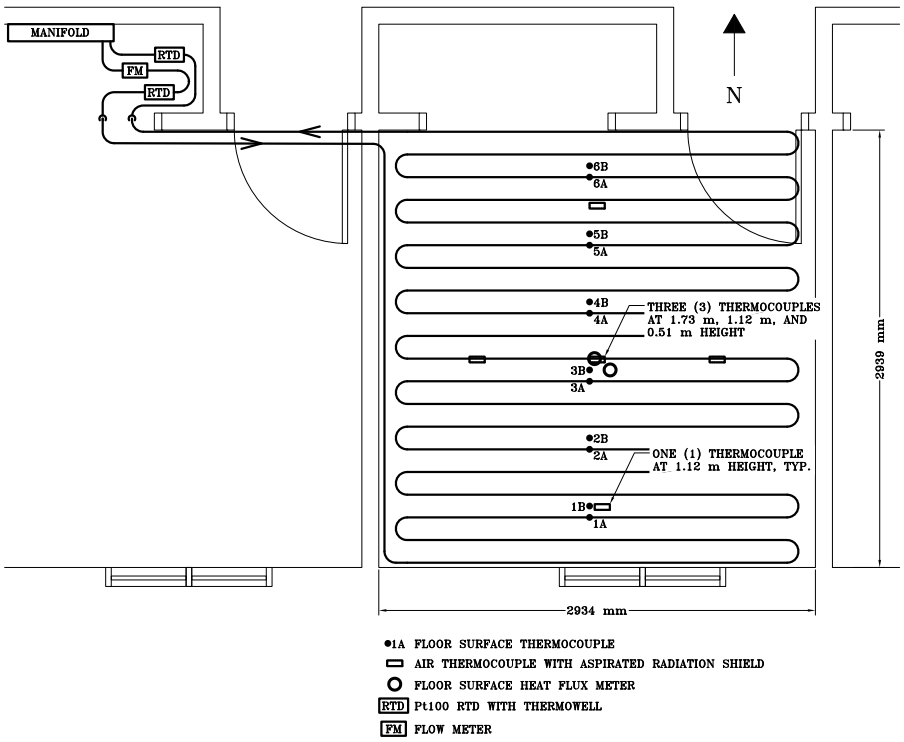


*Figure 3: Plan view of instrumented room with instruments locations (floor plan adapted from drawings by Urbandale Construction)*

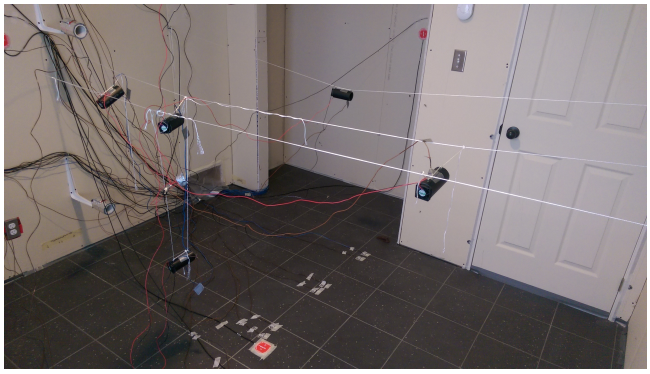

*Figure 4: Picture of instrumented room with aspirated radiation shields, thermocouples, and flux meters*

bration are listed in Table 2. Table 3 shows the total calibration and read/cold junction compensation uncertainty. The uncertainty of the heat flux sensors is 3% while the data acquisition module adds a marginal amount of uncertainty to this error in most cases.
The uncertainty for the measurements was calculated using the method defined by Moffat (1988). The uncertainty $B$ of a single measurement $X$ with multiple sources of errors $j$ is found using Equation 1.

$$B_X = \left\{ \sum_{j=1}^{n} (B_j^2) \right\}^{1/2} \quad (1)$$

Water inlet and outlet temperatures were measured with platinum resistance thermometers (Pt100) in thermowells. Investigations showed that the thermowells had no significant impact on steady state measurements with the Pt100s. Furthermore, the time constant of the thermowell and Pt100 was found to be approximately 23 $s$. Since this is much smaller than the time constant of the floor and the minimum simulation time step, it should not affect the results. A Fluke 1524 reference thermometer was used to read the resistance from the Pt100s. The total uncertainty considering all sources for the Pt100s was 0.03 °C each. The sources of uncertainty for the Pt100s are shown in Table 4.

A Brooks BM02 positive displacement flow meter was used to measure flow rate. The bias error of the flow meter was 1% of measured flow rate. If it is assumed that one pulse is missed or one too many pulses is counted by the data acquisition module, at the end or beginning of the measurement period, this would yield a bias error of 0.00025 $L\,s^{-1}$ or 1% of each individual measurement at every 10 seconds (experiment sampling rate). Figure 5 shows a picture of the second floor manifold for the radiant floor system, as well as the flow meter and Pt100s inside thermowells. The manifold, flow meter, and Pt100s are located approximately 2 $m$ from the room in which the testing is taking place. Some heat will be transferred from the water to the floor in the area in the room adjacent to the test room, however this will be minimal as the section of tubes running in that area were installed

*Table 2: Thermocouple calibration uncertainty sources*

| Bias Error Sources | Regression Residual | Cold Junction Drift | Calibration Reference RTD | Read Error |
|---|---|---|---|---|
| Bias Error Values (°C) | 0.084 | 0.15 | 0.03 | 0.2 |

*Table 3: Thermocouple uncertainty sources*

| Bias Error Sources | Calibration | Experiment Read and CJC |
|---|---|---|
| Bias Error Values (°C) | 0.27 | 0.38 |


*Figure 5: Picture of radiant floor manifolds with temporary flow meter and Pt100s*

without the heat transfer promoting aluminium fins. The heat transfer rate between the water and the floor was calculated with Equation 2.

$$\dot{Q}_{water} = \dot{V}\rho C_p \left(T_{in} - T_{out}\right) \tag{2}$$

The density and specific heat vary with temperature. Data from the CRC Handbook of Chemistry and Physics Haynes (2013) was used to fit sixth order polynomials for both properties. The resulting residuals were negligible. The CRC Handbook of Chemistry and Physics quotes uncertainties of 0.001% and 0.1% for density and specific heat at 1 atm. The bias error from the calculation of the heat transfer rate between the water and the floor was then evaluated by propagating the bias errors of the Pt100s and the flow meter with Equation 3 (Moffat, 1988).

$$B_I = \left\{ \sum_{i=1}^{n} \left( \frac{\partial I}{\partial X_i} B_i \right)^2 \right\}^{1/2} \text{ where } I = f(X_i) \tag{3}$$

Where $X_i$ is measured data used to calculate the derived value $I$ (in this case heat transfer rate).

**Experimental tests**

Tests were performed during the night of May 14th to May 15th, 2016 . A night time test was performed in order to eliminate all solar gains. The elimination of solar gains in the experiment simplifies the simulation and removes uncertainty from modelling of the solar radiation when comparing the AFTP radiant floor model with the experimental results. Although the radiant floors were kept active after sunrise, those data points are ignored for the analysis below. All radiant floors in the house were heated simultaneously to achieve similar temperatures in all zones. The goal was to reduce heat transfer between zones through the walls. Additionally, the door to the test room was kept shut, and an attempt was made to make the room more air tight. No ventilation systems were in use during the test. All windows in the house were shut for the duration of the test. The front door of the house remained sealed for the duration of the test, except for a few seconds within the first 30 minutes of the test to allow the author to leave for the night.

In order to recreate the same type of step input temperature profile as used for the inter-model comparison previously described, a constant temperature water source is required. An electric boiler with a PID controller was used for this purpose. However, the boiler was unable to provide a constant temperature water supply required to create a step input. Nevertheless, the experimental data can still be used and the appropriate boundary conditions can be applied to the model for comparison with the experiment.

Figure 6 shows the inlet, outlet, average floor surface, and average room air temperatures during the test. Figure 7 shows the corresponding top surface heat flux and volumetric water flow rate. Time 0 on the x-axis corresponds to 23:00 in the evening of May 14th. The sampling rate was 10 seconds for all instruments, but continuous lines are shown for clarity.

*Measurement of surface temperature by contact method*

Accurate temperature measurement of a surface surrounded by a gas (or liquid) is problematic. Michalski et al. (2001) describe three sources of error when measuring a surface temperature: The first is caused by the deformation of temperature field due to the temperature sensor. The second is caused by the contact resistance between the temperature sensor (in this case thermocouple bead) and the surface. The third is caused by the distance between the sensitive point of the temperature sensor and the surface being

*Table 4: Pt100 uncertainty sources*

| Bias Error Sources | Sensor | Resistance Measurement | Calibration Fit |
|---|---|---|---|
| Bias Error Values (°C) | 0.02 | 0.02 | 0.008 |

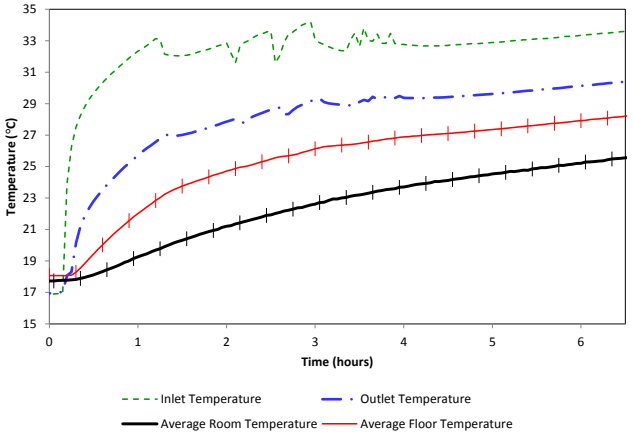


*Figure 6: Experimental data (temperatures)*

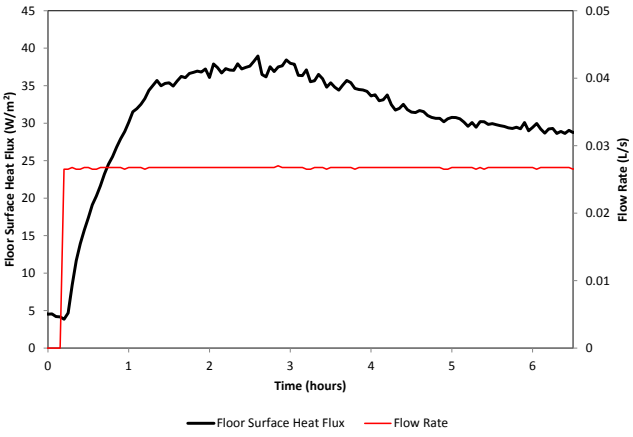


*Figure 7: Experimental data (heat flux and flow rate)*

measured. In all three cases, the greater the difference in temperature between the surrounding fluid and the surface, the greater the error. In the case of the walls and ceiling, this should be a minor issue as the surface temperatures should be close to the air temperature. However, the floor temperature gets much warmer than the air temperature and this can cause a larger error than what is accounted for with typical error analysis.

Moffat proposed a simple correction for surface measurements with thermocouples (Moffat, 2004) as shown in Equation 4. This correction only accounts for the deformation of the temperature field. The results of this correction are discussed later.

$$\frac{T_{measured} - T_{undisturbed}}{T_a - T_{undisturbed}} = \frac{\left(\frac{\sqrt{hD_{bead}k_{wire}}}{2k_{surface}}\right)}{1 + \left(\frac{\sqrt{hD_{bead}k_{wire}}}{2k_{surface}}\right)} \quad (4)$$

where $T_a$ is the air temperature, $T_{undisturbed}$ is the undisturbed floor temperature (to be solved for), $T_{measured}$ is the measured floor temperature, $h$ is the combined convective/radiative heat transfer coefficient, $D_{bead}$ is the thermocouple bead diameter, $k_{wire}$ is the thermocouple wire conductivity and $k_{surface}$ is the floor cover conductivity. Because the convective/radiative heat transfer coefficient is used, it is assumed that the air temperatures and surfaces temperatures (other than the floor) are equal. In reality, the various surface temperatures in the zone were found to be within 1 °C of the air temperature.

**Modelling**

A representation of the test room was created in ESP-r. Although the floor construction was known, the thermal properties of those materials were not. Table 5 shows the material properties used in the model for the floor construction. The joist space between the first and second floor was modelled as a separate zone with the gypsum board layer on the bottom of this zone.

The subfloor (plywood) properties were taken from a building load calculation manual (Spitler, 2010). The insulation conductivity was calculated from manufacturer's data. Other properties were taken from an ASHRAE handbook (ASHRAE, 2009). The thinset mortar was Mapei Ultraflex 3. Properties were taken for cement mortar in a heat transfer textbook (Rathore and Kapuno, 2010) as no data was found for the thinset mortar. It was assumed that the layers of mortar were 0.0032 m thick however this may vary. The cement backing board was a HardieBacker backerboard. The conductivity was taken from the manufacturer (ICC Evaluation Services, 2014). The density and specific heat were estimated based on values found in a ASHRAE handbook (ASHRAE, 2009) however these may vary greatly in reality. The tile density was estimated based on the weight and dimensions. The tile material was porcelain. García et al. (2011) have measured the thermal properties of various types of ceramic tiles including two types of porcelain tiles. The two types of porcelain tiles they measured had densities of 2380 and 2410 $kg\ m^{-3}$. This is higher than the calculated value for the tile installed at the CHEeR facility. However, since this is

*Table 5: Parameters for floor construction in model*

| Material | Thickness $(m)$ | $k$ $(W\ m^{-1}K^{-1})$ | $\rho$ $(kg\ m^{-3})$ | $C$ $(J\ kg^{-1}K^{-1})$ |
|---|---|---|---|---|
| Subfloor | 0.0159 | 0.120 | 540 | 1210 |
| High Density Insulation | 0.0250 | 0.032 | 40 | 1470 |
| Aluminium Fin[a] | 0.0015 | 70.0 | 900 | 880 |
| Thinset Mortar | 0.0032 | 0.72 | 1860 | 780 |
| Cement Backing Board | 0.0064 | 0.2835 | 1300 | 840 |
| Thinset Mortar | 0.0032 | 0.72 | 1860 | 780 |
| Tile | 0.009 | 1.5 | 2089 | 730 |

[a] The thickness of the aluminium layer was tripled in the model due to numerical issues. To account for this, the conductivity and density were divided by three. Since the resistance to conduction is very small in the y-axis, the reduction in conductivity should not affect the model's results.

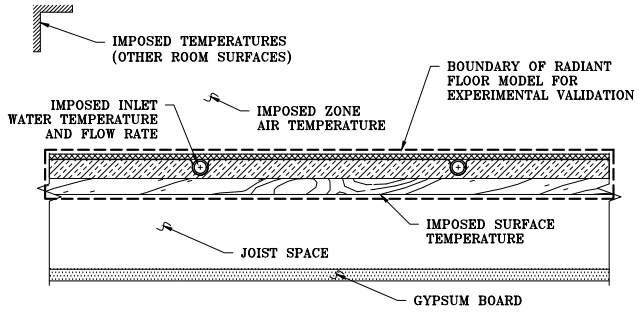


*Figure 8: Boundary conditions applied on model for experimental validation*

the only data available, the specific heat and thermal conductivity of the lighter porcelain tile, measured at room temperature by García et al. (2011) were used. The longwave emissivity of the tile and drywall were measured by Pr. Michael Collins at the University of Waterloo with the use of a Gier Dunkle DB-100 reflectometer. The tile had a hemispheric emissivity of 0.80 and the drywall 0.83. Glass was assumed to have a hemispheric emissivity of 0.87 [1].

The aim of the model discussed earlier in this paper is the calculation of the heat transfer rate between the water and the floor. The ESP-r building domain (one dimensional finite difference model) then calculates the average temperatures at every layer of the floor and the heat fluxes at the top and bottom surfaces. In order to isolate the radiant floor model from the rest of the room model, the measured room air temperature, the various measured walls and ceiling temperatures, and the measured bottom subfloor surface temperature were imposed on ESP-r. These boundary conditions are shown in Figure 8. Imposing these temperatures allowed for the isolation of the radiant floor model from the rest of the room.

[1] Reported values for emissivity of glass vary greatly in the literature. The ASHRAE Fundamentals Handbook (ASHRAE, 2009) reports a value of 0.84, while Clarke (2001) report values as high as 0.937.

In ESP-r, imposing the surface temperatures was accomplished with the use of the existing ESP-r embedded-tube radiant floor model. Each of the surfaces was given a high conductivity and low thermal mass, as well as high flow rate and small tube spacing. The supply temperatures were set to the measured surface temperatures. The room air temperature was imposed to ESP-r by supplying a very large amount of air at the measured air temperature, while maintaining the same convective heat transfer coefficients. The bottom subfloor surface temperature was imposed by supplying a very large amount of air at the same temperature as the measured bottom subfloor surface temperature to the joist space below the floor, and imposing a very large convective heat transfer coefficient to the surface.

**Experiment vs model comparison**

The simulation time step was 3 minutes. As mentioned earlier, the experimental sampling rate was 10 seconds. In order to be able to compare them with the simulated results, only the experimental data corresponding with a 3 minute time interval was considered. Instantaneous values were used as opposed to averages of the previous time interval because the radiant floor model was developed for instantaneous data. Figure 9 shows the location of the top surface heat flux and below subfloor heat flux on a section of floor. The modelled and the experimental results are shown in Figures 10 through 12.

The RMSD of the modelled vs experimental floor surface temperature was 0.54 °C. The RMSD of the top and bottom floor surface heat flux were 2.42 $W\ m^{-2}$ (7.7% of average heat flux of 31.54 $W\ m^{-2}$) and 1.17 $W\ m^{-2}$ (38% of average heat flux of 3.10 $W\ m^{-2}$) respectively. Finally, the RMSD of the water heat transfer rate was 19.5 $W$ (4.0% of average heat transfer of 485 $W$).

As can be seen in Figure 10, the model predicted the heat transfer rate between the water and the floor quite well. There was however an initial under-

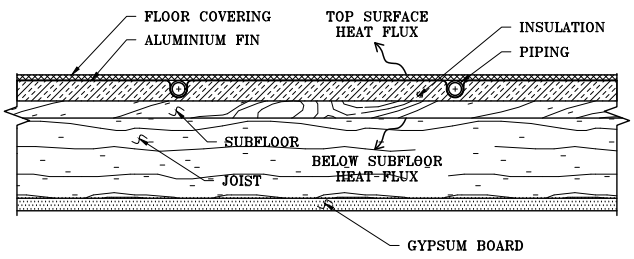


*Figure 9: Location of measured and predicted heat flux surfaces*

prediction for the first few time steps followed by an over-prediction of the heat transfer rate. Following approximately the first hour, the model consistently slightly under-predicted the heat transfer rate, but tended to capture the transient effects relatively well. Most of the data points were not within the experimental error bars.

It is likely that the considerable error seen in the first few time steps is a result of imperfect initial conditions. Varying initial conditions with depth in the floor construction is not possible without source code modifications in ESP-r. Instead, the modelled floor surface initial condition was maintained by controlling the indoor air temperature prior to the beginning of the tests. This did not guarantee that the entire floor layers were at the appropriate temperature however.

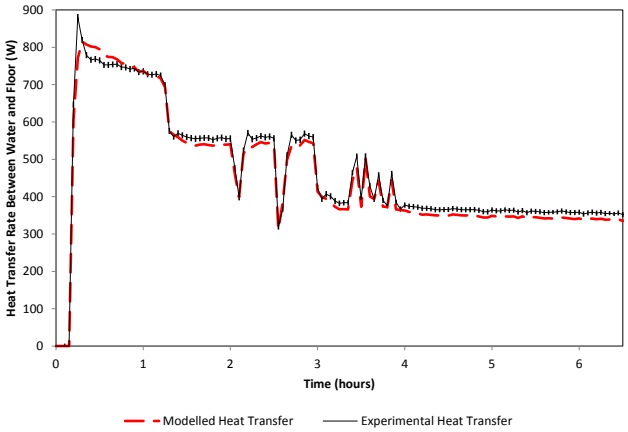


*Figure 10: Experimental vs Modelled Results: Water Heat Transfer Rate*

Figure 11 shows measured floor temperature, as well as the corrected (or undisturbed) floor temperature as per Equation 4. The average value of the right hand side of Equation 4 for the duration of the test was 0.22. This is equivalent to an average difference of 0.83 °C between the undisturbed and measured floor temperatures for the duration of the test. The modelled floor temperature and corrected results seem to agree very well. The modelled air temperature is not shown as the measured experimental values were imposed on the model. The error bars on the uncorrected floor temperature measurements are only shown every 6 time steps for clarity.

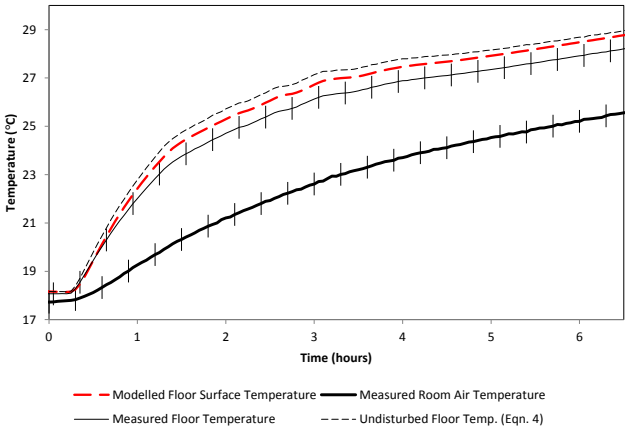


*Figure 11: Experimental vs Modelled Results: Air and Floor Surface Temperature*

Figure 12 shows the surface heat fluxes. As can be noticed, there was a lag between the modelled top surface heat flux and the experimental value at the beginning of the test. This may have been caused by inaccurate model inputs (thermal properties of materials) or it could have been caused because of the simplifications in the model. The latter is however unlikely as the finite element inter-model comparison discussed earlier in this chapter showed no such lag. Most of the modelled points did not fall within the error bars and were under-predicting the experimental results. Additionally, the heat flux below the subfloor was greatly inaccurate when evaluated in terms of percentage error. As mentioned earlier, the RMSD was 38% of the average. In absolute value however, it was very small due to the small amount of heat flux flowing downwards. The error bars for the heat flux from the subfloor are not shown for clarity as they were very small (less than 0.2 $W\ m^{-2}$).

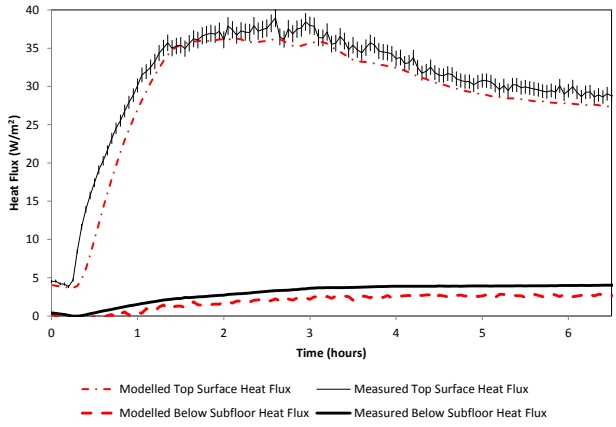


*Figure 12: Experimental vs Modelled Results: Heat Fluxes*

With the parameters described in Table 5, the model under-predicted the heat transfer from the water to the floor, from the top surface to the room, and from the bottom surface to the joist cavity.

**Sensitivity analysis**

As discussed in the Modelling section, many of the floor construction thermal properties were not known, and were approximated with general handbook or textbook data. To investigate the effect of the sensitivity of the model to some of the parameters, additional simulations were run. A *low diffusivity* and a *high diffusivity* case were defined. In the low diffusivity case, the conductivities of the tile and thinset mortar layers was reduced by 10% while the thermal mass of those layers was increased by 10%. For the high diffusivity case, the conductivities of the tile and thinset mortar was increased by 10% and the thermal mass of those layers was reduced by 10%. The model described in the Modelling section was used as the base case.

Table 6 shows the results of the RMSD for the various model outputs. Those results show that the material properties can have an impact on the results, especially for the top surface heat flux. In the following sections, the corrected (or undisturbed) temperature, as defined in Equation 4 is used when discussing the floor temperature.

Not shown in Table 6 is the fact that, similar to the base case, the simulated results for the low diffusivity and high diffusivity cases also under-predicted the heat transfer from the water to the floor, from the top surface to the room, and from the bottom surface to the joist cavity. This can be seen by looking at the percent error of the simulated results in the total energy transferred over the entire test. The total energy transferred is simply the heat flux (in $W\,m^{-2}$) or heat transfer rate (in $W$) integrated over time (to give $J\,m^{-2}$ or $J$). This is shown in Table 7 where a negative value means that the experiment produced a higher energy transfer than the model.

As is seen from the results in Tables 6 and 7, there is not one case that improves all aspects of the model. Additionally, depending on the metric used (percentage error for total heat transfer, or RMSD) one might come to a different conclusion as to which case better predicts the experimental data. The goal of this exercise was to show that a change in material properties by an amount that is within the uncertainty of what is typical in BPS could yield significantly different results.

Similarly, convective heat transfer coefficients have a high level of uncertainty. The convective heat transfer coefficient used for the base case simulation was taken from a correlation by Awbi and Hatton (Awbi and Hatton, 1999). This is just one of many heat transfer correlations available for a heated floor with buoyancy driven heat transfer. A sensitivity analysis was conducted to study the sensitivity of the heat transfer coefficient on both tests. The other convective heat transfer coefficients investigated were formulated by Alamdari and Hammond (Alamdari and Hammond, 1983) and Khalifa and Marshall (Khalifa and Marshall, 1990). Figure 13 shows the convective heat transfer coefficients $h_{conv}$ for a range of difference in temperature between the floor surface and the air ($\Delta T$) for the three correlations. The figure is for a 3 $m$ by 3 $m$ room.

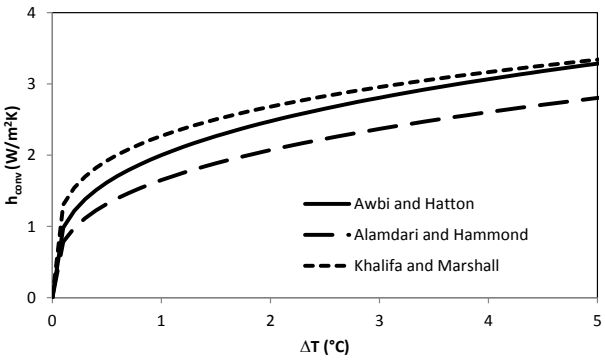


*Figure 13: Comparison of convective heat transfer coefficient correlations over range of $\Delta T$ in tests*

Table 8 shows the RMSD between the experiment and the model with the various convective heat transfer coefficients (Awbi and Hatton is the base case). Table 9 shows the percentage error for the total energy transferred (water to floor, floor to room, subfloor to joist space) over the entire test period associated with the heat transfer coefficients. In Table 9, a negative value shows that the experiment produced a higher energy transfer than the model. The choice of heat transfer coefficient seems to have some impact on the accuracy of the model. In this case, the Khalifa and Marshall correlation gave results that are in closer agreement with the measured data. That correlation also happened to give higher heat transfer coefficients in the range of $\Delta T$ encountered in the test discussed here. Because the Khalifa and Marshall model produces higher heat transfer coefficients, it may artificially counteract the suboptimal choices of material properties as input to the model. Therefore, it should not be thought as the more accurate correlation.

## Conclusion

In this paper, an experiment to validate an above-floor tube-and-plate radiant floor model is presented. RMSD between the experiment and the model for top surface heat flux was 2.42 $W\,m^{-2}$ (7.7% of the average top surface heat flux). The percentage error of the total energy transferred at the top surface was 5.9%. Similarly, the RMSD for the heat transfer between the water and the floor construction was 19.5 $W$ (4.0% of the average heat transfer rate). The percentage error of the total energy transferred between the water and the floor was 2.5%.

*Table 6: Material sensitivity - RMSD*

| | Average Experiment Value | RMSD: Experiment vs Model | | |
|---|---|---|---|---|
| | | Base Case | Low Diffusivity | High Diffusivity |
| Temperature Top Floor Surface (°C) | 26.3 | 0.29 | 0.39 | 0.21 |
| Heat Flux Top Surface ($W\ m^{-2}$) | 31.5 | 2.42 | 3.05 | 2.01 |
| Heat Flux Bottom Surface ($W\ m^{-2}$) | 3.10 | 1.17 | 0.99 | 1.29 |
| Water to Floor Heat Transfer ($W$) | 485 | 19.5 | 19.6 | 20.3 |

*Table 7: Material sensitivity - Percentage error for total energy transfer*

| | Model Percentage Error (%) | | |
|---|---|---|---|
| | Base Case | Low Diffusivity | High Diffusivity |
| Heat Flux Top Surface | -5.9 | -8.2 | -4.0 |
| Heat Flux Bottom Surface | -37 | -31 | -41 |
| Water to Floor Heat Transfer | -2.5 | -1.9 | -2.9 |

*Table 8: Convective heat transfer coefficient sensitivity- RMSD*

| | Average Experiment Value | RMSD: Experiment vs Model | | |
|---|---|---|---|---|
| | | Awbi and Hatton | Alamdari and Hammond | Khalifa and Marshall |
| Temperature Top Floor Surface (°C) | 26.3 | 0.29 | 0.17 | 0.33 |
| Heat Flux Top Surface ($W\ m^{-2}$) | 31.5 | 2.42 | 3.05 | 2.28 |
| Heat Flux Bottom Surface ($W\ m^{-2}$) | 3.10 | 1.17 | 1.08 | 1.19 |
| Water to Floor Heat Transfer ($W$) | 485 | 19.5 | 24.5 | 18.5 |

*Table 9: Convective heat transfer coefficient sensitivity - Percentage error for total energy transfer*

| | Model Percentage Error (%) | | |
|---|---|---|---|
| | Awbi and Hatton | Alamdari and Hammond | Khalifa and Marshall |
| Heat Flux Top Surface | -5.9 | -8.5 | -5.3 |
| Heat Flux Bottom Surface | -37 | -34 | -37 |
| Water to Floor Heat Transfer | -2.5 | -3.8 | -2.1 |

It was found that the model was sensitive to construction thermal properties; the percentage error of the predicted amount of energy transferred from the water to the floor varied between 2.9% and 1.9% for high and low diffusivity floor construction cases. The convective heat transfer coefficient also affected the model results. The total water to floor total energy transferred percentage error varied between 3.8% and 2.1% when switching between the Alamdari and Hammond and the Khalifa and Marshall correlations.

## Acknowledgement

The authors would like to acknowledge the support of the NSERC Smart Net-Zero Energy Buildings Research Strategic Network, the Ontario Graduate Scholarship Program, and the J.Y. and E.W. Wong Research Award for their financial support.

## References

Alamdari, F. and G. P. Hammond (1983). Improved data correlations for buoyancy-driven convection in rooms. *Building Services Engineering Research and Technology 4*(3), 106–112.

ASHRAE (2009). *2009 ASHRAE Handbook: Fundamentals*. Atlanta, USA: American Society of Heating Refrigerating and Air-Conditioning Engineers.

Athienitis, A. and Y. Chen (2000). The effect of solar radiation on dynamic thermal performance of floor heating systems. *Solar Energy 69*(3), 229–237.

Awbi, H. and A. Hatton (1999). Natural convection from heated room surfaces. *Energy and Buildings 30*(3), 233–244.

Brideau, S. and I. Beausoleil-Morrison (2014). Model Development for Tube-in-Subfloor Radiant Floor Heating and Cooling. In *eSim2014*, Ottawa.

Brideau, S. A., I. Beausoleil-Morrison, M. Kummert, and A. Wills (2016). Inter-model comparison of embedded-tube radiant floor models in BPS tools. *Journal of Building Performance Simulation 9*(2), 190–209.

Cho, S.-H. and M. Zaheer-uddin (1997). Temperature regulation of radiant floor heating systems using two-parameter on-off control: An experimental study. *ASHRAE Transactions 103*(1), 966–982.

Clarke, J. A. (2001). *Energy Simulation in Building Design* (2nd ed.). Oxford: Butterworth-Heinemann.

García, E., A. de Pablos, M. Bengoechea, L. Guaita, M. Osendi, and P. Miranzo (2011). Thermal conductivity studies on ceramic floor tiles. *Ceramics International 37*(1), 369–375.

Haynes, W. (Ed.) (2013). *CRC Handbook of Chemistry and Physics* (94th ed.). Boca Raton, USA: CRC Press. Section 6-1.

ICC Evaluation Services (2014). Legacy Report: NER-405. Technical report.

Johnson, G. (2011). Design and commissioning of an experiment to characterize the performance of a lithium-bromide absorption chiller. Master's thesis, Carleton University.

Kattan, P., K. Ghali, and M. Al-Hindi (2012). Modeling of under-floor heating systems: A compromise between accuracy and complexity. *HVAC & R Research* (July), 37–41.

Khalifa, A. J. N. and R. H. Marshall (1990). Validation of heat transfer coefficients on interior building surfaces using a real-sized indoor test cell. *International Journal of Heat and Mass Transfer 33*(10), 2219–2236.

Laouadi, A. (2004). Development of a radiant heating and cooling model. *Building and Environment 39*(4), 421–431.

Michalski, L., K. Eckersdorf, J. Kucharski, and J. McGhee (2001). *Temperature Measurement* (Second ed.). Chichester, UK: John Wiley & Sons.

Moffat, R. J. (1988). Describing the uncertainties in experimental results. *Experimental Thermal and Fluid Science 1*(1), 3–17.

Moffat, R. J. (2004). *CRC Handbook of Mechanical Engineering* (Second ed.). Boca Raton, USA: CRC Press. Section 4.6.

Rathore, M. M. and R. Kapuno (2010). *Engineering Heat Transfer* (Second ed.). Sudbury, USA: Jones & Bartlett Learning.

Spitler, J. D. (2010). *Load Calculation Applications Manual* (SI ed.). Atlanta, USA: ASHRAE.

Tarara, J. M. and G.-A. Hoheisel (2007). Low-cost Shielding to Minimize Radiation Errors of Temperature Sensors in the Field. *42*(6), 1372–1379.

Yeo, M. and K. Kim (1997). A Study on the Thermal Performance Simulation to Evaluate the Prefabricated Radiant Floor Heating Panels. In *Proceedings of the 5th International IBPSA Conference*, Prague, Czech Republic.